Deformation of mineral crystals in cortical bone depending on structural anisotropy

Bijay GIRI [a], Shigeru TADANO [a]*, Kazuhiro FUJISAKI [a], Naoki SASAKI [b]

[a] Division of Human Mechanical Systems and Design, Graduate School of Engineering, Hokkaido University, Sapporo, Japan

[b] Department of Biological Sciences, Graduate School of Science, Hokkaido University, Sapporo, Japan

* Corresponding Author:

Shigeru TADANO, PhD

Professor, Division of Human Mechanical Systems and Design, Graduate School of Engineering, Hokkaido University

N13 W8, Kita-ku, Sapporo 060-8628, Japan

Tel/Fax: +81-11-7066405

E-mail: tadano@eng.hokudai.ac.jp

Word count (revised manuscript): 276 (Abstract); 4054 (Introduction through Conclusion)

Abstract

The deformation mechanism of bone at different hierarchical levels has been of wide interest. The important features of bone, its anisotropy and orientation dependent deformation are equally important, which have also gained a long run discussion. Most of the studies are concentrated on protein-rich collagen fibres and matrix, where different deformation mechanisms at the lower length scales are proposed. But in relation to this, how the mineral particles behave depending on their distribution is yet to be revealed in detail. In the present work, we demonstrate mineral crystals deformation and arrangement characteristics on the basis of experimental outcomes. Using X-ray diffraction procedures, we quantified the mineral strains, degree of orientation of the crystallites and their evolution under different applied step-loads in bovine femoral cortical specimens having different alignment with the femoral axis direction. We provide a direct quantitative comparison of these parameters in the specimens having preferential orientations roughly at 0, 30, 45, 75 and 90 degrees with reference to the loading direction. The mineral strains in the compliant specimens, i.e. 0 and 30 degrees oriented specimens were observed to differ with the stiffer specimens, i.e. 75 and 90 degrees oriented specimens, whereas the 45 degrees oriented specimen show almost equal strains at different loads. These were explained by the degree of orientation with reference to the loading direction and the preferential orientation direction of the specimens. On the basis of observed parameters, we describe deformation phenomena of mineral particles to occur in different stages, which consist of redistribution stage, elastic strain stage and inelastic strain stage. These phenomena are expected to occur at different scales and rates depending on the orientation and distribution of crystals.

Keywords:

mineral strain; structural anisotropy; degree of orientation; crystallites evolution; X-ray diffraction

Introduction

The structure-property-function relationship in bone has been of wide interest to the investigators, the proper knowledge of which will unfold many issues of clinical relevance regarding bone fracture risks. But this has appeared rather complex because of diverse behaviour of bone in different structural levels [1]. The basic building block of bone, minerals and proteins, show different characteristics, while the highly enhanced mechanical behaviour of bone composite has been generally accepted attributing to the presence of minerals in the collageneous matrix at smaller length scales [2]. The hydroxyapatite crystallites are brittle with low tensile strength, whereas the protein-rich collagen fibres are tough and fairly strong in tension; this combined structure gives bone both high strength and high toughness. However, their mutual interaction is still under discussion [3,4].

The nanoscale deformation in bone governed by two-phase structure of collagen-mineral composite has received increased attention. Borsato and Sasaki [5] was the pioneer on using weaker X-rays to calculate changes in crystals lattice spacing to describe internal stresses in bone. Recently, high energy X-rays has been used to quantify mineral phase stresses [6], collagen fibril strains [7], and cooperative deformation of mineral and collagen phases [8,9]. Application of weaker X-ray source has also been emphasized with new analysis methods concentrating the case of bone [10,11]. Where the collageneous matrix is considered crucial in dissipating energy with strain-controlled failures [12], the geometrical arrangement of mineral particles is also considered equally important for optimized mechanical performance [13-14]. The toughness of bone composite is further said to be by virtue of glue type sacrificial bonds available in collagen matrix [15-17]. Hence, considerable progress has been achieved

related to the deformation characteristic of collagen fibres and matrix, but detail on the mineral particles behaviour and their role is still lacking.

The mineralized structure is highly anisotropic. These crystals are found to grow with a specific crystalline orientation, the c-crystallographic axes (i.e., *002*-lattice plane) of which are said to be parallel to the long axes of collagen fibres. The presence of such mineral crystals within the fibres makes it different from other composite materials. The mechanical loading would affect the material bone differently in different hierarchies; it might be different for different lamella to the crystal grains. Hence, the deformation of bone as a whole is not only controlled by the fibrils characteristics, but how minerals respond is also important. With the proposal of bone as a two-phase composite of mineral reinforced collagens [18], discussions on the anisotropic properties of bone continued to the range of orientations of bone axes with stress axes [19-22], microstructures [23] or fracture toughness and crack propagation [12,24].

In the present work, we report for the first time a quantitative comparison of deformation mechanism of mineral crystals and their structural anisotropy. A laboratory based X-ray diffraction system was used to investigate cortical bone specimens from bovine femoral shaft. To provide a direct comparison of the extent of crystals, defined as the degree of orientation (DO) here, crystallites evolution and the strains developed in the minerals, we used five types of specimens having different preferential alignments with the femoral axis. Different parameters were quantified and compared in these compliant and stiffer specimens during tensile loads applied at different steps.

Materials and methods

Specimen

A fresh bovine femur was obtained and frozen at -30^{o}C. Mid diaphyses with approximate length of 50 cm was cut for further preparation. The mid shaft was again divided into two longitudinal halves to harvest specimens of different orientation to the femoral axis (Fig. 1). Specimens along the femoral axis (roughly at 0 degree) and roughly at 30 degrees were obtained from one of the halves; specimens of roughly 45 degrees, 75 degrees and 90 degrees (transverse) were obtained from another half. The inclination angles were decided visually. First, the bone was cut in the widths of 5 mm at different orientations; these were then cut into the strips to obtain the final specimens. Size of all the final specimens were approximately 45 mm long and 0.5 mm thick (except 90 degrees specimen, which was little shorter). Rough cuts were done using hand-saw and fine cuts using diamond circular blade with continuous irrigation of water.

Strain gages were glued almost at the middle of the specimens to record the applied strains. The specimens were stored in a closed pack when not in use to avoid dehydration. The samples were allowed to dry during the exposure of X-rays only. The differently oriented specimens each was used in the diffraction study and the mechanical tests. Because of high measurement precision, all the specimens were prepared from the same femur diaphyses to avoid variation of crystallites distribution characteristics in different sources.

Diffraction experiment and analysis

RINT2000 X-ray diffraction system (Rigaku Co., Japan) was used to generate X-rays with characteristics Mo-Kα, Mo target, wave length 0.071 nm, tube voltage 40 kV and tube current 40 mA. The specimen was mounted to a screw-driven tensile loading device with its length along the loading direction. The beam was irradiated perpendicular to the specimen next to the strain gage with the collimator of diameter 1 mm for 10 minutes. The transmitted intensity was detected by the imaging plate (BAS-SR 127 mm × 127 mm, Fuji Photo Film Co. Ltd., Japan). The specimen was placed at a distance 157 mm from the source. R-axis DS3C scanner (Rigaku Co., Japan) was used to readout the intensity data detected by the imaging plate to obtain two-dimensional diffraction patterns at 50 μm/pixel resolutions. Representative diffraction patterns are shown in Fig. 2. Step-loads were applied to the specimens starting at the strain gage reading of approximately 1500 microstrains ($\mu\varepsilon$) and increased at the steps of 500 $\mu\varepsilon$ till the specimens fractured. The diffraction images at no-load and loaded conditions were taken thrice at each step, hence providing the total combination of nine datasets in all the cases. Corresponding readings of the load-cell in the device were also noted. Both the readings of the strain gage (termed as tissue strain in the article) and the load-cell (termed as tissue stress after calculating with cross section area) were recorded immediately before and after the exposure to note any significant slippage at the mountings.

The beam centre was determined using software R-axis (compatible with the scanner) enveloping the diffraction region of *211*- and *002*-planes. The intensity patterns were converted to the Cartesian distribution (diffraction angle '2θ' as abscissa and intensity values '*I*' as ordinate) by binning the pixel intensity data in the azimuthal

(β) steps of 0.1 degree to obtain 3600 radial-line distributions. The radial distributions were obtained by the weighted-average of intensities as described elsewhere [11]. The binning was performed for *211*- and *002*-diffraction regions over radial ranges of 60 and 55 pixels respectively. Diametrically opposite peaks were added to get the diameter of the ring. Lattice strains at *211*- and *002*-diffraction planes were calculated at different azimuthal angles using the peak at full-width half-maximum (FWHM) as described elsewhere [11] to obtain 1800 strain distribution data. A simple moving average was performed for the width of 10 data and the strain distribution was truncated to 0.5 degree intervals.

All the analyses of the diffraction patterns were performed using a software program developed in our laboratory. Experiments were carried out under nearly the identical environmental conditions maintained within the generator (temperature = 23.8 ^{o}C; relative humidity = 48 %).

Degree of orientation

The reflection of *002*-plane is often used to characterize the orientation pattern of apatite crystals. The dense arc-shaped intensity region of *002*-plane in the diffracted intensity pattern (Fig. 2) provides the estimate of orientation distribution of crystallites c-axes. Here, we quantified the two-dimensional distribution function of crystals in terms of Herman's Orientation Function (HOF), defined as Degree of Orientation (DO). HOF is a relatively simple mathematical expression, which gives the extent of orientation of the crystals (i.e. the degree of orientation) as a single quantified value with respect to a reference direction. It can be expressed as follows:

$$DO = \frac{3 < \cos^2 \beta > -1}{2} \quad (1)$$

The parameter $<\cos^2\beta>$ is expressed as [25]:

$$< \cos^2 \beta >= \frac{\int_0^{\pi} I(\beta) \cos^2 \beta \sin \beta d\beta}{\int_0^{\pi} I(\beta) \sin \beta d\beta} \quad (2)$$

Here, I(β) is the intensity at azimuths β. Hence,

$DO \rightarrow 1$ (if orientation $\rightarrow$ reference direction),

$DO \rightarrow$ - 0.5 (if orientation $\rightarrow$ perpendicular to reference direction),

$DO \rightarrow 0$ (if orientation is random).

Intensities along the radial lines within the annular area enveloping *002*-plane over the radial range of 55 pixels were azimuthally integrated at 0.1 degree intervals. Because of symmetry, only one-half of the diffraction data were used. The minimum intensity of the azimuthal scan was then deducted from the total integrated values, which would give I(β) for Eq. (2). The integrated intensity profiles along *002*-plane for the specimens at no-load is shown in Fig. 2. The *DO* is quantified with reference to the loading direction ($\beta = 0^o$) and preferential oriented directions of the specimens, where the considered direction is reference for the variation of β in Eq. (2).

Mechanical testing

The real time macroscopic deformations in differently oriented specimens were also observed in the Instron (Model 4411, USA). The specimens were mounted by aligning the longer axis vertically and loaded under tensile loading at the strain rate of 0.1 % s^{-1} till they got fractured.

Results

A representative azimuthally integrated intensity profile of 002-plane at no-load condition is shown in Fig. 2. The differently aligned specimens named as S00, S30, S45, S75 and S90 have preferential orientations 6.6, 26.4, 43.5, 75.3 and 83.1 degrees respectively with the loading direction. Stress values were obtained from the loading device and strain values from the strain gage glued to the specimens. Internal strains, i.e. mineral strains, were calculated from the X-ray diffraction data. During the application of external loads at the steps of 500 $\mu\varepsilon$ starting at 1500 $\mu\varepsilon$, S30 failed at increasing the load after 2500 $\mu\varepsilon$, S45 failed after 3000 $\mu\varepsilon$, S75 failed after 2000 $\mu\varepsilon$ and S90 failed after 1500 $\mu\varepsilon$. S00 was found to withstand the load considerably above 3000 $\mu\varepsilon$. The corresponding tissue stresses observed were 95.7, 70.3, 61.9, 45.5 and 32.0 MPa respectively for S00, S30, S45, S75 and S90. The slippages at the mountings were checked by calculating difference in the strains and loads observed in the strain gage and load-cell respectively. The mean difference percentages are listed in Table 1. Except for S90, no significant differences were observed.

Polar diagrams of mineral strains from *002*- and *211*-planes at different step-loads are shown in Fig. 3. The orientation distributions obtained from the azimuthal integrated intensity of *002*-plane are also plotted. The horizontal and vertical loops represent

tensile and compression regions respectively. Mineral strains along the loading direction at different load steps together with corresponding tissue stresses are shown in Fig. 4. The tissue deformation for all the specimens is linear (except S90); hence indicating they were in the elastic range before fracture. The Young's modulus were obtained to be 24.7, 20.2, 16.4 and 15.5 GPa for S00~S75 respectively. For S00, mineral strain along the loading direction is closely linear up to 2500 $\mu\varepsilon$ applied load, and shows decreased value after that. The deformations per applied macroscopic strain for S30 and S45 have also gradually decreased. S45 shows almost equal mineral strains at different loads. S75 and S90 show comparatively larger strains; for S75 the minerals are further observed not to deform at the increased load step of 2000 $\mu\varepsilon$. The mineral strains from *002*-plane are larger compared to *211*-plane for all the specimens; the difference is more for S90. The strains measured after the load is released (or after the fracture) are also plotted. Approximately -1500 $\mu\varepsilon$ is observed to remain in S45 and 2000 $\mu\varepsilon$ in S90 for *002*-plane; for other specimens, the strains after unloading are approximately ±500 $\mu\varepsilon$. The strains after unloading from *211*-plane are found to be in the range of -160~600 $\mu\varepsilon$ among the specimens.

Herman's orientation function, expressed as the degree of orientation (DO) with reference to the loading direction and preferentially orientated direction of the crystallites are plotted in Fig. 5. The DOs along the loading direction represents the amount of crystallites distribution corresponding to the variation of β with reference to the loading direction, whereas the DOs along the preferentially oriented direction are obtained corresponding to the variation of β with reference to the respective preferential orientation of the crystallites in the specimens. The DOs along the loading direction (Fig. 5 (top)) have obvious variation from approximately 0.5 for S00 to -0.3 for S90 showing

the crystallites distribution concentrating away from the loading direction gradually with the increasing alignment of the specimens (see Fig. 2 also). The values at different step-loads in the case of S00 for both loading and preferentially oriented directions are mostly close, whereas they are different for other specimen cases because of distinct variation of loading direction and preferential aligned direction. For S30, the DOs corresponding to the loading direction have increased with the increasing loads, but decreased corresponding to the preferentially oriented direction. S45 shows gradual decrease along the preferentially oriented direction. After unloading, the crystallites are observed to concentrate more along the preferentially oriented direction except for S90.

The evolution of crystals, represented by FWHM of radial distributions at different azimuthal angles of *002*-plane, are shown in Fig. 6. For S00 and S30, decrease in radial widths due to the loads is observed along the loading direction. For S45, the radial widths are almost equal indicating slight or no evolution of the crystals. For S75, the evolution of crystals along the preferentially orientated direction i.e., close to 75 degrees is observed to occur at larger extent, whereas for S90, it is different. S90 shows decreased radial width along the loading direction in larger scale.

Discussion

For long bones like femur, the mineral crystals have distinct textures, which can be simply quantified by azimuthally integrating the intensity of *002*-plane. Considering different femoral cortical samples, we quantified the internal strains obtained from crystallites deformation and other parameters to characterise their distribution, namely degree of orientation and its evolution, to illustrate the orientation affected deformation characteristics in bone tissue.

The comparatively uniform distribution of strain for *211*-plane in Fig. 3 is expected since they are obtained from the diffraction of inclined planes, which provides almost uniformly distributed diffraction ring because of larger number of participating planes compared to *002*-plane. The *002*-plane represents c-axis orientation and consists of the crystallites alignment directly. Thus, the strain distributions from *002*-plane show that the minerals are not deformed azimuthally uniformly under the loads. The uniformity in the distribution decreases with the increase of off-axis loads; it is more pronounced for 45 degrees alignment. Furthermore, from the strain distribution loops we can see that S00 has significant tension and compression loops, whereas S45 possesses majorly compression loops; rest of the specimens lack distinct compression. At the lower load of 1500 $\mu\varepsilon$, S00 shows smaller tensile region than compression, and this increases with increasing loads. This can be regarded to the resistance of mineral crystallites initially to the loads acting along their alignment direction, and hence is different from other specimen cases.

The varying trends in the internal strain behaviour can be explained from the quantified degree of crystallites (DO) along two reference directions, the loading and preferentially oriented directions (Fig. 5). The significant variations in the DOs at the increased loads for S30 are S45 imply that redistribution of the crystals have occurred significantly, because of which there is decrease in the gradient of mineral strains at different loads (Fig. 4). The mineral deformation was not observed for S00 and S75 at the increased load. This could be attributed to the disruption of filaments within the mineralized fibrils capable to reform [17], but possibly by different mechanisms. Because of reforming effect, they bounce back after removing the load as could be observed in their strain values after unloading. For S75, such decrease in mineral strain

is more pronounced possibly because of fewer shears and higher scale disruption, ultimately affecting the distribution of crystals in larger extent. But, what we can see is that, it is still being reformed. The case is different for S90, where the strain at the load is comparatively very high (approximately 5500 $\mu\varepsilon$ in *002*-plane at the applied load of 1500 $\mu\varepsilon$), and has not regained after unload. This is because after less redistribution of the crystals, the interfibrillar bonds go ultimate failure resulting in no reforming or rebounding effect. This can be well observed in the DO after unload and corresponding larger strain (2000 $\mu\varepsilon$) that has remained. For other cases, the DOs after unloading have been regained providing the evidence that the crystals have almost reformed back on releasing the loads. The higher DO is due to increased concentration of the crystals. The extent of crystallites i.e., DOs, we quantified here from the transmitted intensity through the specimens also incorporate the expected range of crystallites orientation distribution in the examined region due to possible twisted plywood organization of collagen fibres as described by Giraud-Guille [26].

To see if there is any significant effect due to strain rate in the diffraction experiment, we also performed tensile test of the specimens at relatively low strain rate of 0.1 % s^{-1}. The specimens were obtained from the locations adjacent to those used in the diffraction studies maintained under identical environment. The stress-strain relations of S30~S90 indicate that fractures had occurred within the elastic limit (Fig. 7). Different parameters obtained from the macroscopic deformation data of diffraction experiments and the mechanical tests are listed in Table 2. It is to be noted that the values of diffraction experiments are immediately before the next step of load at which the fractures occurred; S00 was not tested till the failure. The Young's moduli obtained from both the experiments do not have significant variation. The longitudinal and

circumferential Young's moduli of the specimens, i.e. 24.7 GPa (S00, diffraction) and 18.4 GPa (S90, Instron) are close to previously reported values [10] (27.9 and 19.6 GPa respectively).

The FWHM of radial distributions within certain width of *002*-plane provides the change in crystals orientation due to load (Fig 6). Comparing with other observations (Fig. 4&5), we can find the evidence that reorientation or rearrangement of the crystals has occurred for S45 to a larger extent, whereas distinct separation of the crystals have occurred in S90. The azimuthal variation of *002*-intensity also provides the information about uniformity or graininess of the crystal structure. The effect of external loads on the overall crystal structure has been presented as standard deviations of intensity distributions and diametrical widths of *002*-plane (Fig. 8). Considerable changes in the *002*-widths with loading are observed in the specimens except S45. Such change has remained in S00 after unloading as well.

Thus, we observed here that the differently oriented crystallites experienced varying deformations along loading direction. S00 and S30 have crystallites oriented close to the femoral axis and can be regarded as elastically compliant along the loading direction, whereas S75 and S90 have crystallites oriented perpendicular close to the femoral axis and can be regarded as elastically stiff along the loading direction. Here we find smaller strains for S00 and S30 compared to S75 and S90 during identical loading case (Fig. 4). The reason for which has been attributed to the crystallites distribution and evolution (Fig. 5&6). Based on these observations, summarizing the deformation of all the anisotropy cases (Fig. 9) we describe the deformation characteristics of crystals to occur basically in following stages.

From Fig. 9 (top), we can observe three distinct regions; with the increment of internal strains a rapid increase of DO initially followed by almost a constant region and a steeper increment region further at the end. At the first stage, the crystals undergo internal redistribution by reorientation or rearrangement, and at this stage no observable deformation will occur. The degree of such redistribution depends on their initial orientation with respect to the loading direction. It increases with the increase of orientation direction with the loading direction; we assume the optimum being at 45 degrees. Further to this, the degree of redistribution decreases, and is less pronounced than initial case with a very low or almost none near to 90 degrees. At the next stage, the actual deformation occurs resulting in observable strains, which we define as the elastic strain range. The deformation at this stage may take place according to different mechanisms, either by the tension-shear effect [13,14] or increase in gap region within collagen fibrils [27] or due to extension of rebounding sacrificial bonds [15-17]. All of these effects further depend on the crystallites orientation with respect to the loading direction. This is within the elastic range, since the strains are recovered after load release even though the internal strains are not linear as observed here for S00 (Fig. 4). The deformation by these mechanisms occurs easily and is more pronounced for orientation closer to the loading direction. At the third stage, the major deformation occurs in the matrix causing ultimate disruption or failure of the interfibrillar bonds, which is comparatively high and not totally recoverable. This stage is considered as inelastic strain stage, the later part of which will show almost none or low mineral deformation due to permanent breaking up of the bonds. Although it is obvious that the partition of load among minerals, fibrils and matrix differ for all these orientation cases, based on our observation we conclude that for 45 degrees alignment the first stage

deformation occurs mainly, for 0 degree alignment second stage is predominant, where the load is mainly used to produce strains. For 90 degrees alignment third stage is predominant, where the strain produced will initially be higher and non-recoverable. However, all of these stages will be followed by all the orientation types, but at different scale and rate depending on their distribution and alignment with the loading direction. Furthermore, from Fig. 9 (bottom), we can observe that the widths of radial profiles have decreased with the increase in internal strains, which indicates that the strains are resulted mainly due to rearrangement of the crystallites.

We also calculated the Poisson's ratio for tissue deformations and, minerals *002*- and *211*-plane deformations (Fig. 10). Poisson's ratio for tissue deformation is calculated by accounting the longitudinal and transverse deformations measured by the strain gauge, and mineral deformations were calculated by considering the deformation of Debye rings. The tissue deformations have mean value of 0.297 with standard deviation of 0.016 (individual Poisson's ratios are listed in Table 2). The mineral deformations for S45 shows gradual increment of Poisson's ratio (*002*-plane) with the load, however the values and the deviations are high. For others, the mineral deformations are unpredictable. The SEM images of fracture surfaces are also shown (Fig. 11). A longitudinal pull out could be observed in the osteon for S30. In S45, cleavage due to dominant interfibrillar shear is observed. The pull-out faces are fewer because of fibrils and matrix separation in S90.

In this study, the experiments were not performed in buffer solution environment. But due consideration was taken to avoid dehydration in the specimens during the procedures to have less impact on the results.

Conclusion

It is well understood that to describe the macroscopic level characteristics from the microscopic level information, detailed understanding of the response of compositional constituents to the mechanical behaviour is necessary. The long debate on the anisotropic properties and deformation mechanism of two-phase bone composite were basically focused on the nature of protein-rich collagens; although the mineral phase has been recognized to be equally important. For anisotropic composites like bone, the orientation of crystallites with respect to the loading direction determines the degree of compliance or stiffness, and hence the deformations experienced will vary. From a set of crystallites amount, we provided here experimentally based insights on the deformation behaviour of mineral crystals dependent on structural anisotropy. The outcomes of this study will provide new insights on the prevailing issues of bone fractures and risks, and contribute to the medical science by providing better way of assessment of current therapies. Such findings with complex bone tissue will serve as a model for biomimetic materials and aid in the development of novel bio-inspired and nano-composite materials and devices. The current work is also another step forward towards our aim of devising methodologies and developing useful techniques that could be ultimately applied with living bone tissues in clinical practice making use of weaker X-rays.

Acknowledgements

This work was supported by Grant-in-Aid for Scientific Research (A), MEXT (No. 19200035).

5

References

[1] Weiner S, Wagner HD. The material bone: structure-mechanical function relations. Annu. Rev. Mater. Sci. 1998; 28:271-298.

[2] Fratzl P, Gupta HS, Paschalis EP, Roschger P. Structural and mechanical quality of the collagen-mineral nano-composite in bone. J. Mater. Chem. 2004; 14:2115-2123.

[3] Fritsch A, Hellmich Ch. 'Universal' microstructural patterns in cortical and trabecular, extracellular and extravascular bone materials: micromechanics-based prediction of anisotropic elasticity. J. Theor Biol 2007; 244:597-620.

[4] Currey JD. Collagen and the mechanical properties of bone and calcified cartilage. In: Fratzl P, editor. Collagen. New York: Springer; 2008; 397-420.

[5] Borsato KS, Sasaki N. Measurement of partition of stress between mineral and collagen phases in bone using X-ray diffraction techniques. J. Biomech. 1997; 30:955-957.

[6] Almer JD, Stock SR. Internal strains and stresses measured in cortical bone via high-energy X-ray diffraction. J. Struct. Bio. 2005; 152:14-27.

[7] Gupta HS, Wagermaier W, Zickler GA, Aroush DR, Funari SS, Roschger P, Wagner HD, Fratzl P. Nanoscale deformation mechanisms in bone. Nano Lett. 2005; 5:2108-2111.

[8] Gupta HS, Seto J, Wagermaier W, Zaslansky P, Boesecke P, Fratzl P. Cooperative deformation of mineral and collagen in bone at the nanoscale. Proc. Natl. Acad. Sci. USA 2006; 103:17741-17746.

[9] Almer JD, Stock SR. Micromechanical response of mineral and collagen phases in bone. J. Struct. Bio. 2007; 157:365-370.

[10] Fujisaki K, Tadano S. Relationship between bone tissue strain and lattice strain of Hap crystals in bovine cortical bone under tensile loading. J. Biomech. 2007; 40:1832-1838.

[11] Tadano S, Giri B, Sato T, Fujisaki K, Todoh M. Estimating nanoscale deformation in bone by X-ray diffraction imaging method. J. Biomech. 2008; 41:945-952.

[12] Nalla RK, Kinney JH, Ritchie RO. Mechanistic fracture criteria for the failure of human cortical bone. Nature Mater. 2003; 2:164-168.

[13] Jäger I & Fratzl P. Mineralized collagen fibrils: a mechanical model with a staggered arrangement of mineral particles. Biophys. J. 2000; 79:1737-1746.

[14] Gao H, Baohua J, Jäger IL, Arzt E., Fratzl P. Materials become insensitive to flaws at nanoscale: lessons from nature. Proc. Natl. Acad. Sci. USA 2003; 100:5597-5600.

[15] Thompson JB, Kindt JH, Drake B, Hansma HG, Morse DE, Hansma PK. Bone indentation recovery time correlates with bond reforming time. Nature 2001; 414:773-776.

[16] Currey J. Sacrificial bonds heal bone. Nature 2001; 414:699.

[17] Fantner GE, Hassenkam T, Kindt JH, Weaver JC, Birkedal H, Pechenik L, Cutroni JA, Cidade GAG, Stucky GD, Morse DE, Hansma PK. Sacrificial bonds and hidden length dissipate energy as mineralized fibrils separate during bone fracture. Nature Mater. 2005; 4:612-616.

[18] Currey JD. The relationship between the stiffness and the mechanical content of bone. J. Biomech. 1969; 2:477-480.

[19] Bonfield W, Grynpas MD. Anisotropy of the Young's modulus of bone. Nature 1977; 270:453-454.

[20] Katz JL. Anisotropy of Young's modulus of bone. Nature 1980; 283:106-107.

[21] Sasaki N, Ikawa T, Fukuda A. Orientation of mineral in bovine bone and the anisotropic mechanical properties of plexiform bone. J. Biomech. 1991; 24:57-61.

[22] Currey JD, Brear K, Zioupos P. Dependence of mechanical properties on fibre angle in narwhal tusk, a highly oriented biological composite. J. Biomech. 1994; 27:885-897.

[23] Liu D, Wagner HD, Weiner S. Bending and fracture of compact circumferential and osteonal lamellar bone of the baboon tibia. J. Mater. Sci. Mater. Med. 2000; 11:49-60.

[24] Peterlik H, Roschger P, Klaushofer K, Fratzl P. From brittle to ductile fracture of bone. Nature Mater. 2006; 5:52-55.

[25] Wilchinsky ZW. Measurement of orientation in polypropylene film. J. Appl. Phys. 1960; 31:1969-1972.

[26] Giraud-Guille MM. Twisted plywood architecture of collagen fibrils in human compact bone osteons. Calcif. Tissue Int. 1988; 42:167-180.

[27] Sasaki N, Odajima S. Elongation mechanism of collagen fibrils and force-strain relations of tendon at each level of structural hierarchy. J. Biomech. 1996; 29:1131-1136.

Supplementary Material

Click here to download Supplementary Material: legends.doc

Table 1

Difference (%) in strain-gage and load-cell readings during X-rays exposure

Applied strain ($x10^{-6}$)	1500		2000		2500		3000	
	Strain	*Load*	*Strain*	*Load*	*Strain*	*Load*	*Strain*	*Load*
SP00	2.85	1.82	1.25	0.70	1.15	0.40	1.55	0.72
SP30	2.41	2.21	0.48	0.85	0.63	0.48	-	-
SP45	1.90	2.10	0.75	0.79	0.57	0.61	0.90	0.84
SP75	4.12	3.67	2.34	1.47	-	-	-	-
SP90	17.23	5.00	-	-	-	-	-	-

Table 2

Deformation parameters in diffraction and mechanical tests

	Preferential orientation	Stress at failure		Strain at failure		Young's modulus		Poison's ratio
		Diffraction	Instron	Diffraction*	Instron	Diffraction	Instron	
	(degrees)	*(MPa)*		*($x10^{-6}$)*		*(GPa)*		
SP00	6.6±1.1	95.7**	-	3000**	-	24.7	-	0.31±0.02
SP30	26.4±1.5	70.3	84.7	2500	3961	20.2	21.0	0.33±0.02
SP45	43.5±2.7	61.9	60.5	3000	3068	16.4	21.1	0.25±0.01
SP75	75.3±2.4	45.5	41.4	2000	2112	15.5	18.9	0.27±0.00
SP90	83.0±1.3	32.0	36.7	1500	2063	-	18.4	0.38±0.00

* Strain after which fractures occur before next load-step
** Fracture did not occur for S00

Figure(s)

Figure 1 (Giri *et al.*)

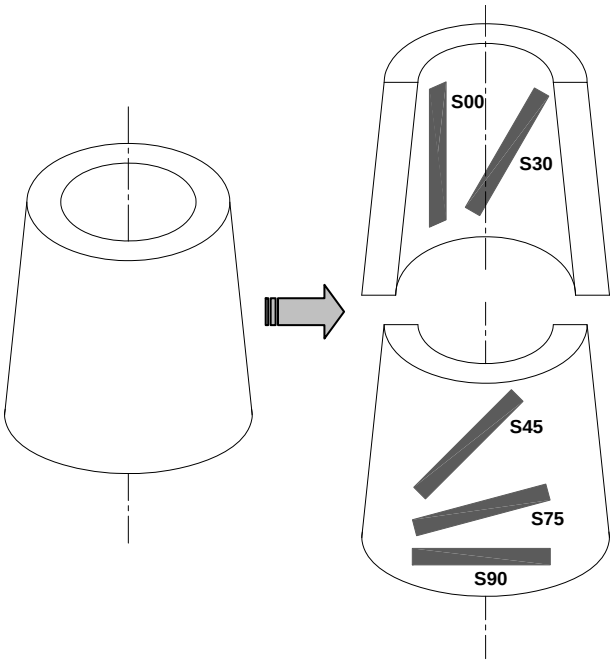

Figure 2 (Giri *et al.*)

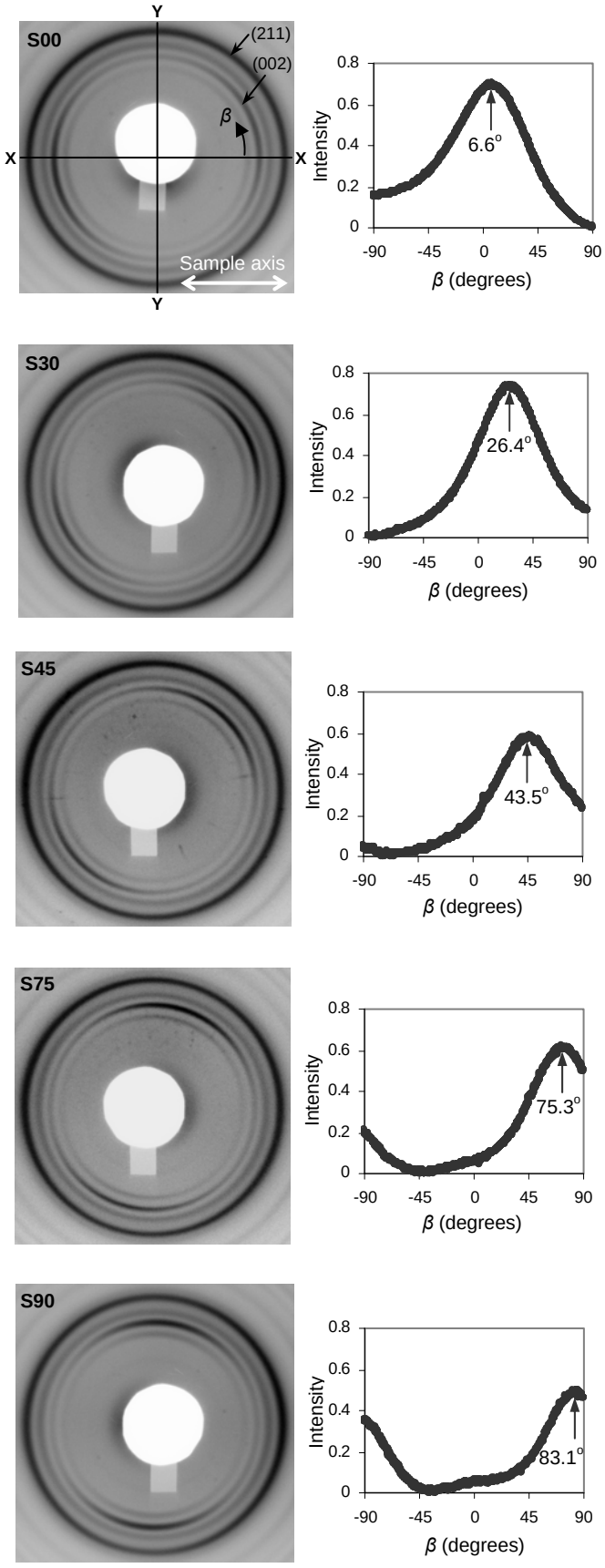

Figure 3 (Giri *et al.*)

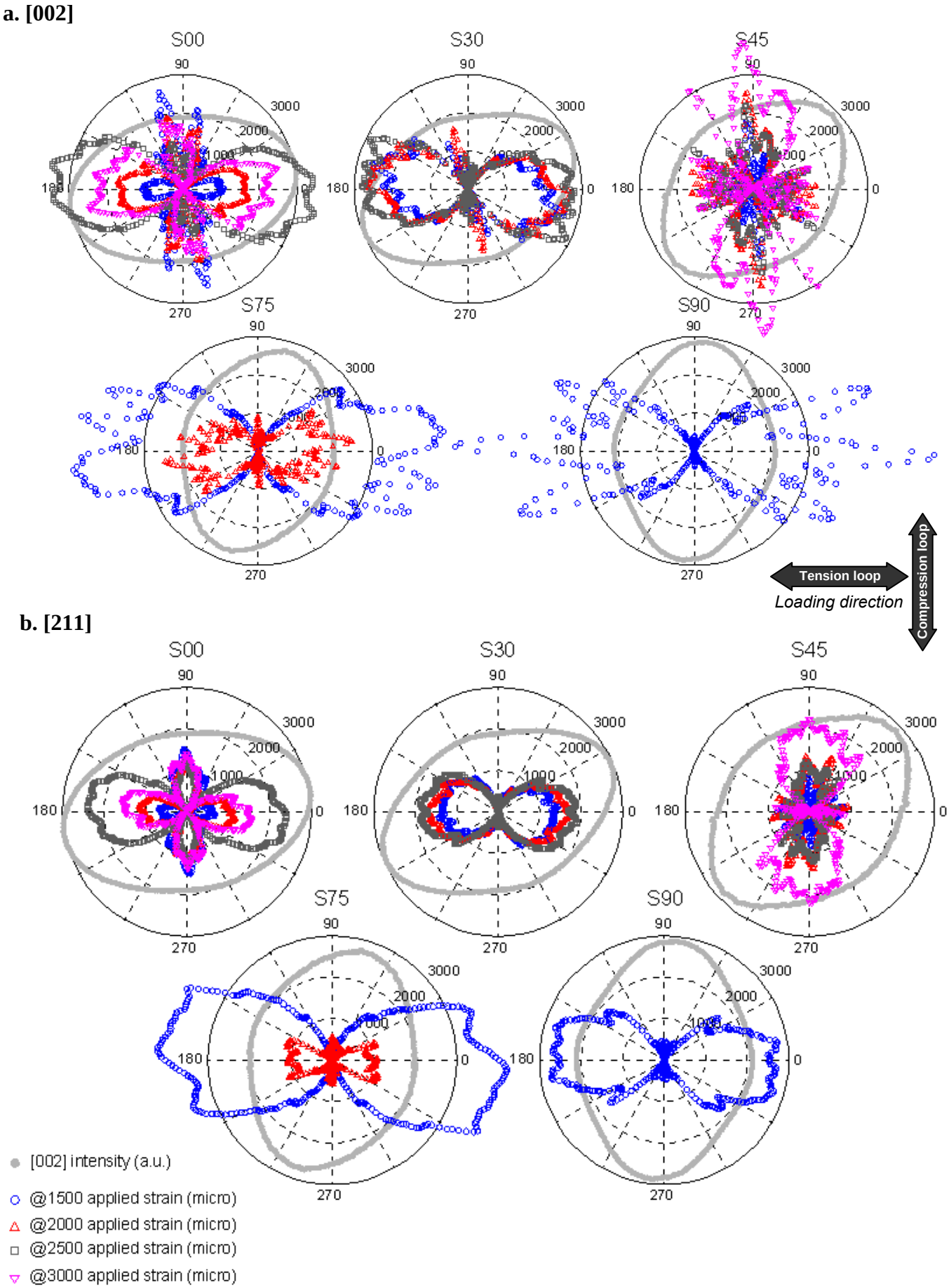

Figure 4 (Giri *et al.*)

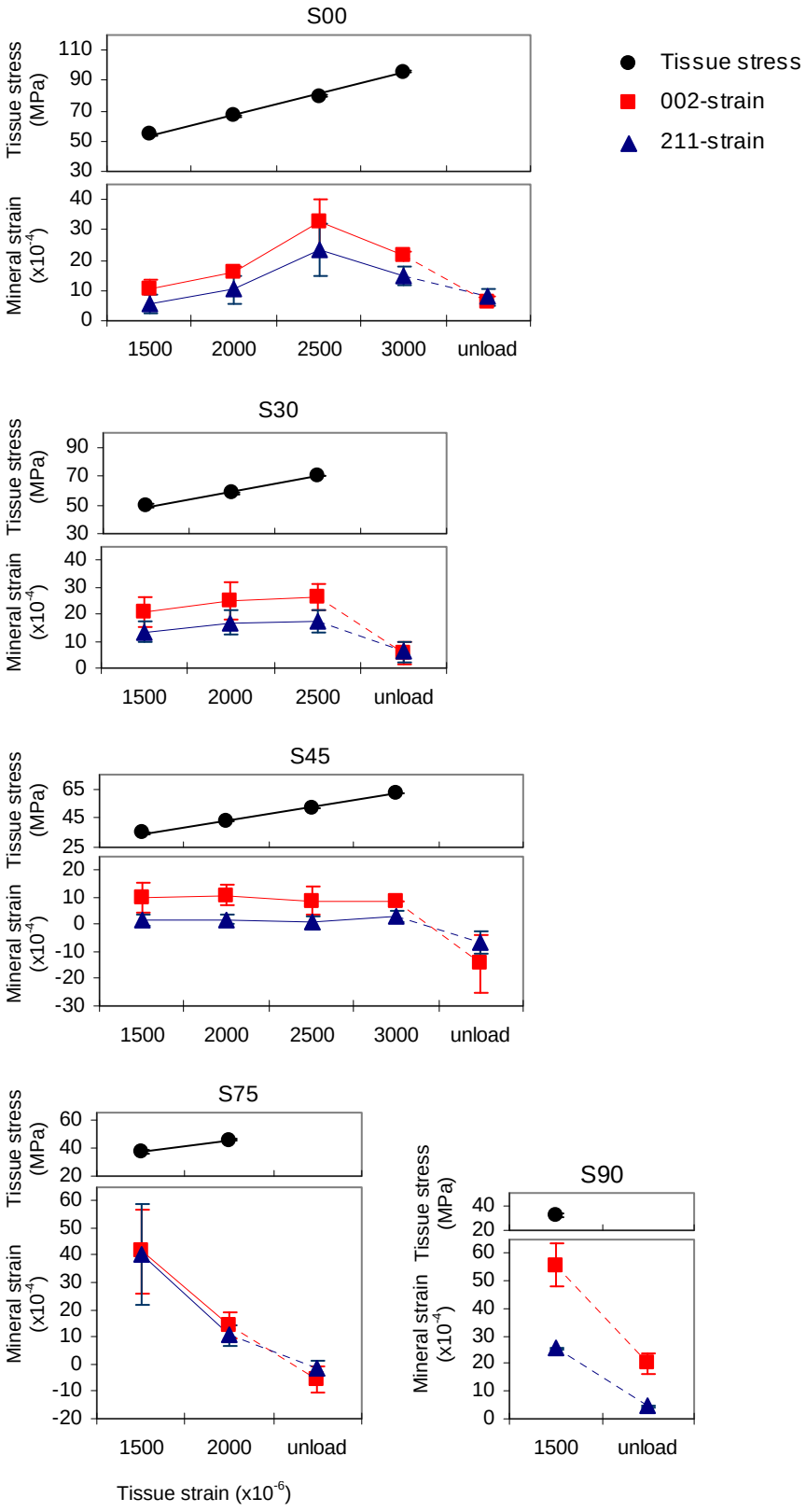

Figure 5 (Giri *et al.*)

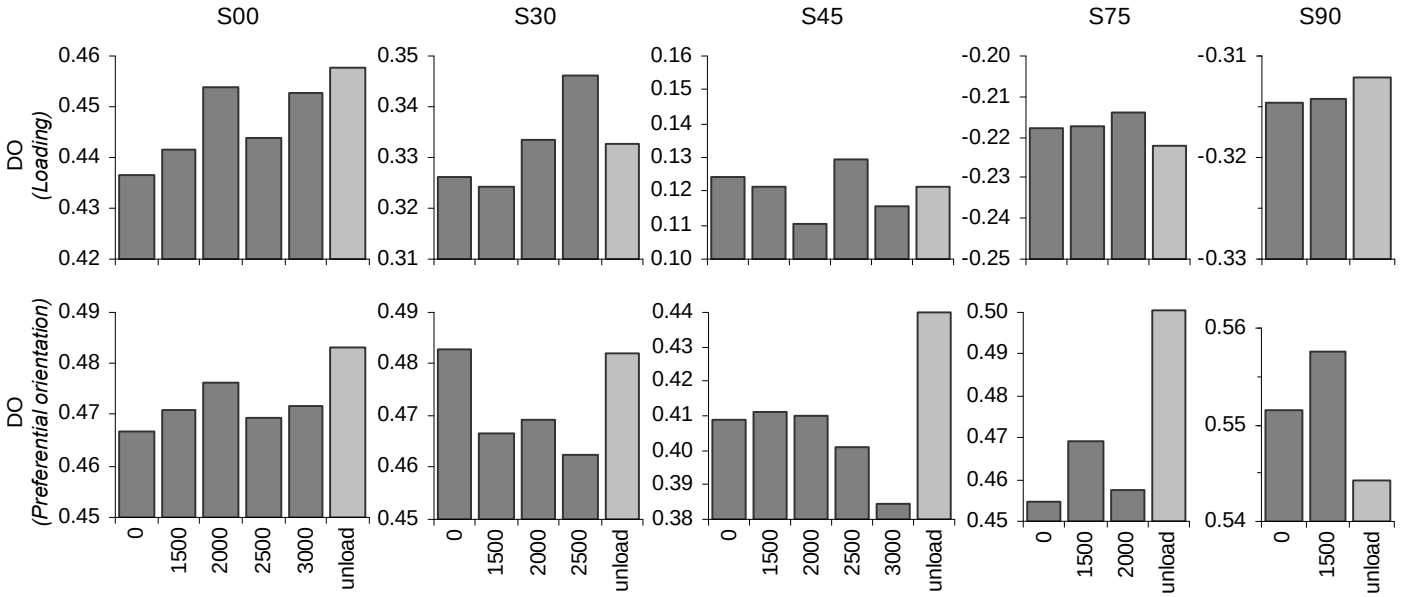

Figure 6 (Giri *et al.*)

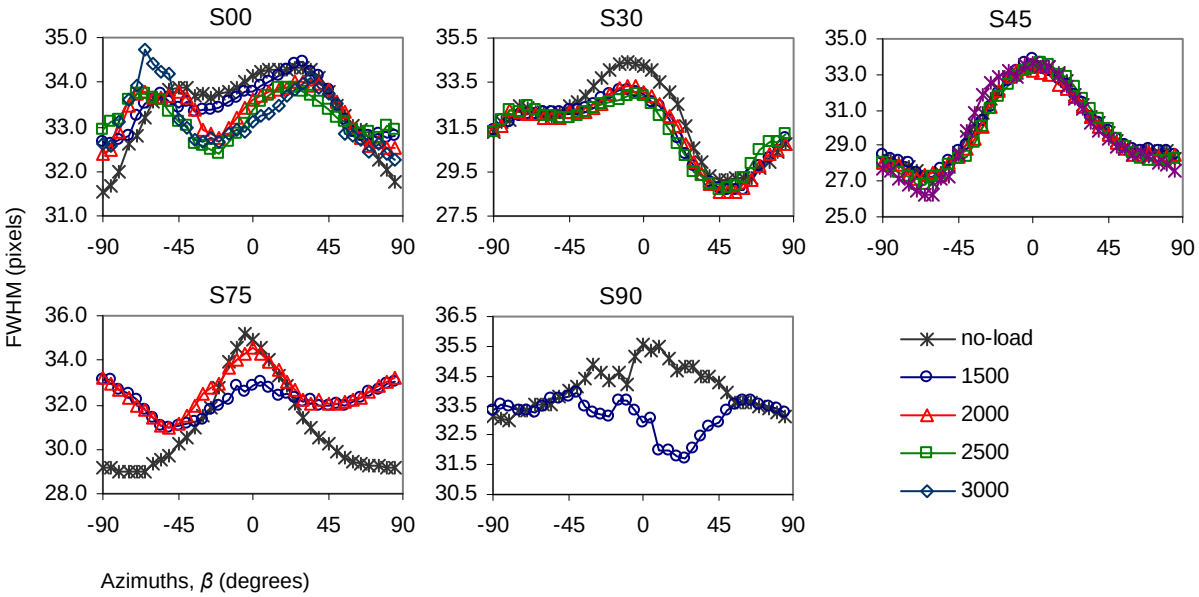

Figure 7 (Giri *et al.*)

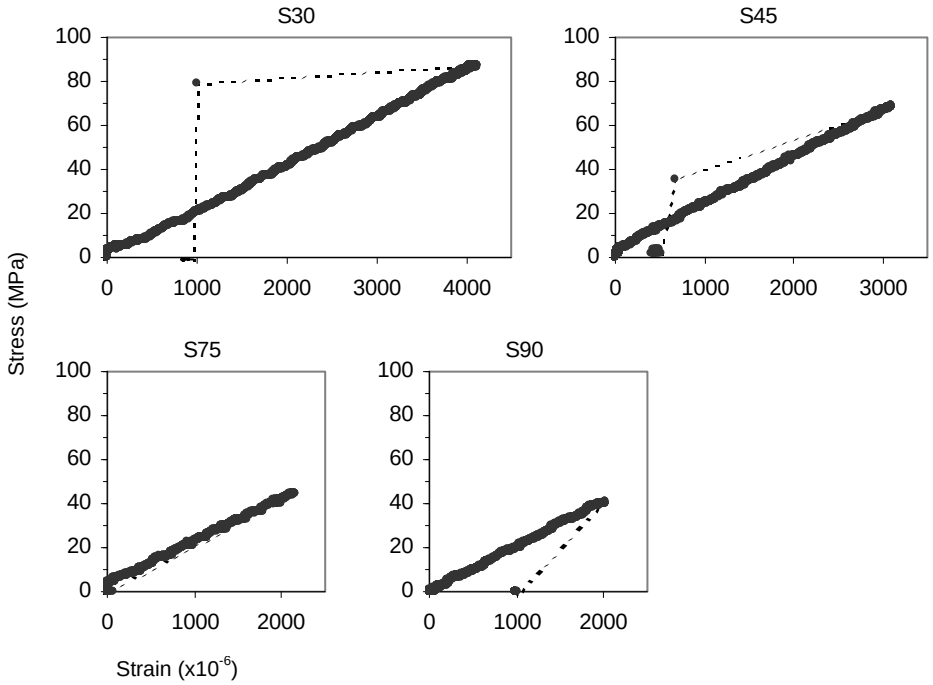

Figure 8 (Giri *et al.*)

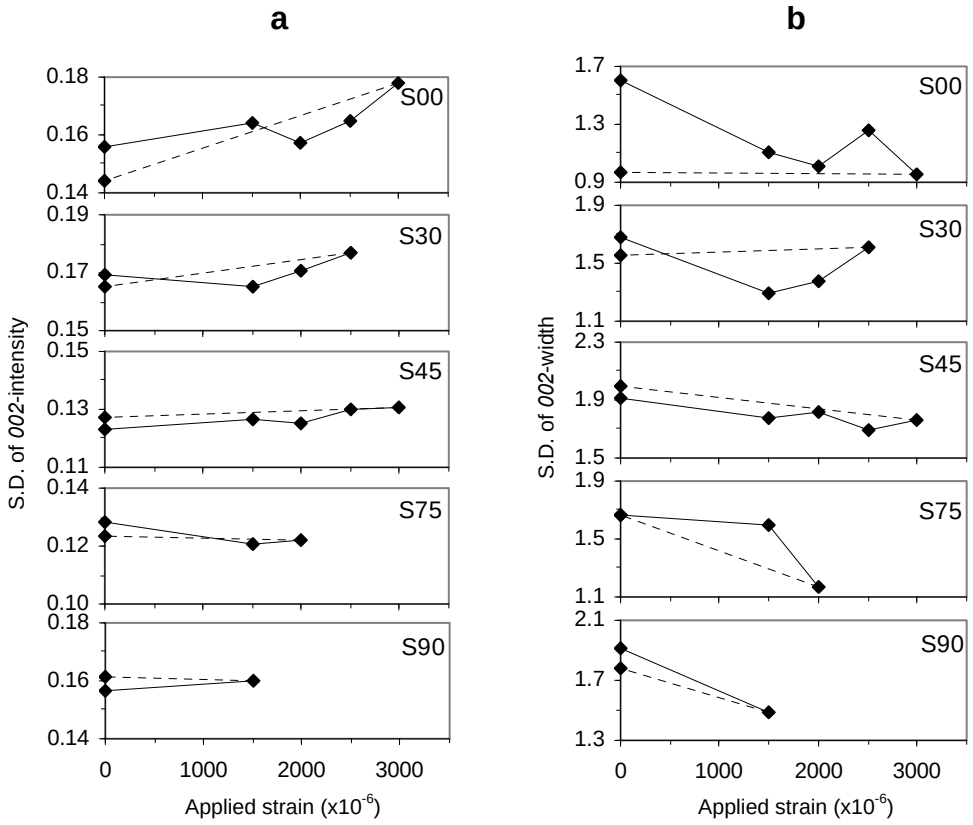

Figure 9 (Giri *et al.*)

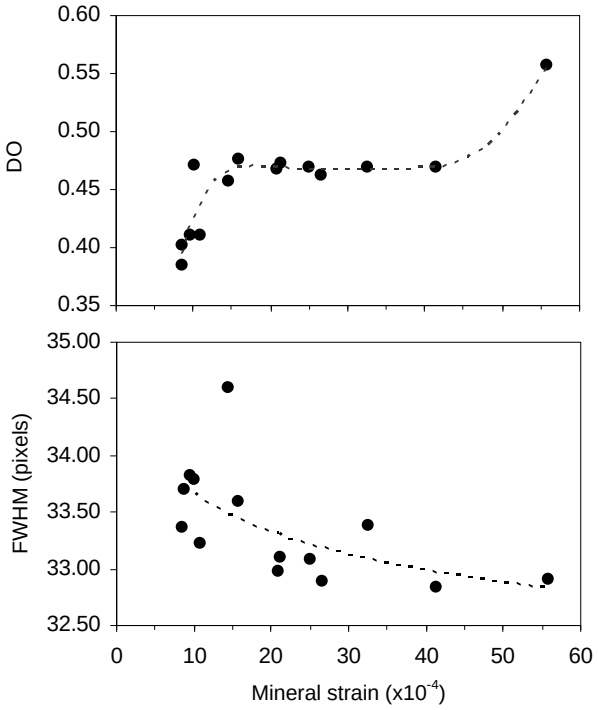

Figure 10 (Giri *et al.*)

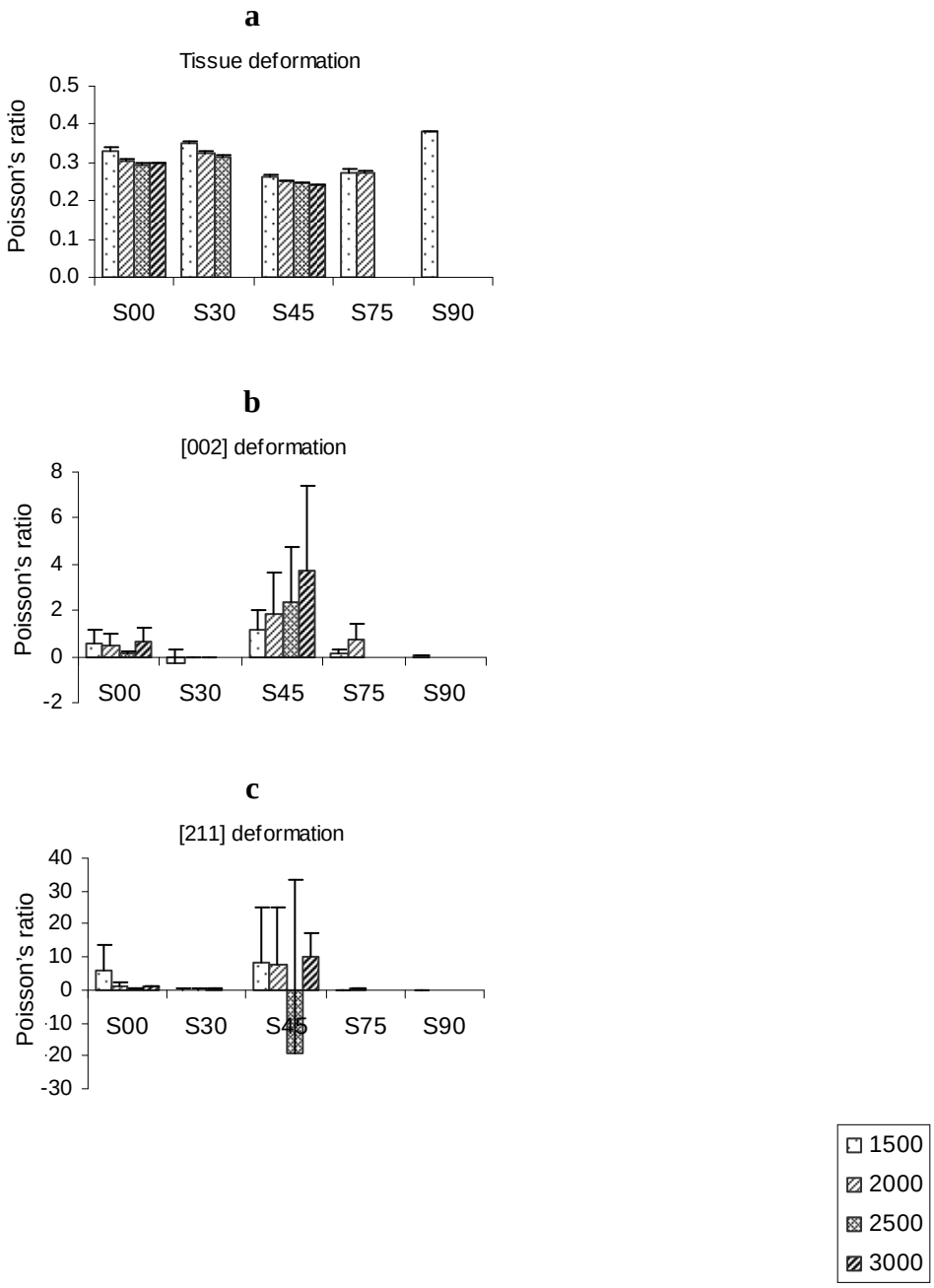

Figure 11 (Giri *et al.*)

a

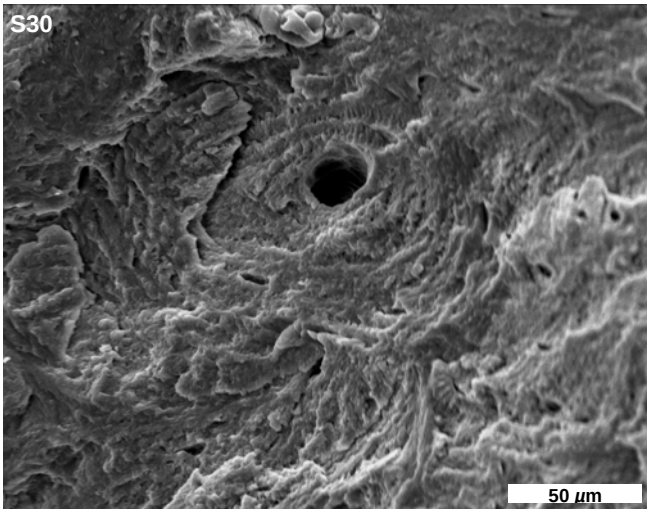

b

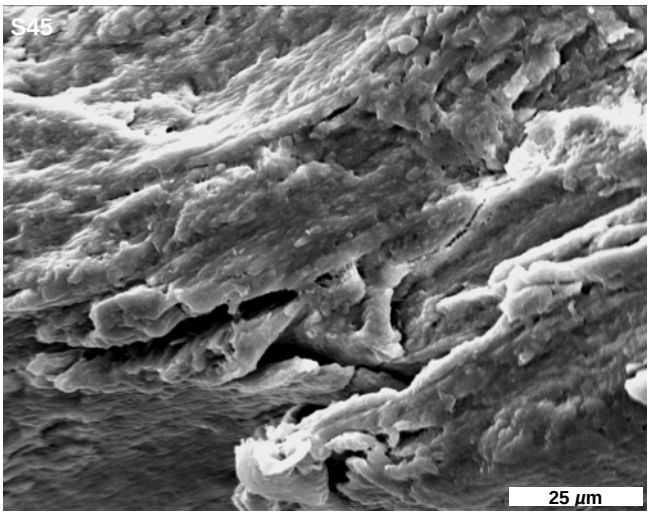

c